Control of STATCOM in Wind Power Plants based on Induction Generators during Asymmetrical Grid Faults

P.Rodriguez*, A.Luna*, G. Medeiros**, R. Tedorescu***, and F. Blaabjerg***
* Technical University of Catalonia
** Federal University of Pernambuco
*** Aalborg University

***Abstract*--This paper explores different strategies to set the reference current of a STATCOM under unbalanced grid voltage conditions. The aim of the proposed control strategies is to provide a set of reactive current references to be injected by the STATCOM under unbalanced grid faults. Their performance, as well as their grid support capability will be evaluated by means of simulations. Finally, the experimental response will be tested in a low-scale setup, in order to verify and validate their dynamic performance and steady state response.**

***Index Terms*-- Electrical engineering, Electric power, FACTS, Power conversion, Reactive power control.**

I. INTRODUCTION

Power electronics systems offer new ways for controlling reactive power in both high-voltage transmissions and low-voltage distribution systems. Reactive power control allows both regulating the voltage level in transmission systems, for maintaining a stable operation of the power system, and compensating particular loads, to improve the supply and demand quality in such loads [1].

Last advances in power semiconductors have aroused the Static Synchronous Compensator (STATCOM) as an effective solution that overcomes the limitations of the Static Var Compensators (SVC) in medium-voltage distribution systems. The STATCOM generally uses a voltage source converter (VSC) to accurately regulate the reactive current injected into the grid terminal, which allows injecting full rated current almost independently of the system voltage level [2]. Moreover, the STATCOM offers an excellent dynamic performance in controlling reactive power [3]. All these features, plus high efficiency and small footprint, make the STATCOM a very suitable solution to increase the operational efficiency and stability of power systems [4], to mitigate the effects caused on the grid by fluctuating loads as arc furnaces [5], to achieve fast and accurate voltage regulation at critical loads [6] and to satisfy reactive current requirements regarding the grid connection of distributed generators [7].

This work was supported by the project ENE2008-06841-C02-01/ALT. The authors would like to recognize the support of CAPES and CNPq.

The STATCOM's manufacturers have gained a remarkable share in the market of electrical equipments for wind farms in the last years. This is due to the fact that the STATCOM has demonstrated to be a powerful solution to allow certain wind turbines (WT) to agree with the strict grid connection rules imposed by the transmission system operator (TSO), in countries with large-scale integration of wind power [8]-[10]. The effectiveness of the STATCOM in improving both, the transient response and the low voltage ride through capability, of wind farms based on induction generators (IG) and doubly fed induction generators (DFIG) has been reported in [11]. Considering that IG based wind farms still represent a significant 30% of the installed wind power in Europe [12], enhancing their Fault Ride Through (FRT) capability is necessary in order to improve the power system stability [13], [14].

In all these works, it is demonstrated that the STATCOM action enhances the performance of the wind farm when affected by balanced voltage sags. These studies match to that stated in the grid code requirements, since almost all the grid codes in force set requirements considering balanced voltage conditions, and just short comments are made regarding wind farm performance during unbalanced faults [8][10]. However, in practice more than 90% of the grid faults result in unbalanced voltages sags. In [15], it was demonstrated that a properly controlled STATCOM might independently compensate the positive- and negative-sequence components of unbalanced voltage sags

.

This paper studies different strategies for determining the reactive current to be injected by the STATCOM during unbalanced grid faults. Taking into account the switching frequency limitations in real applications, the strategies under analysis will provide 50Hz sinusoidal reference signals, that can be easily tracked with standard current controllers. The reactive power injection capability of the STATCOM is evaluated in each case, as well as its capability to boost the voltage at the point of common coupling (PCC), and hence to improve the wind turbines operation.

II. IG-WTS UNDER VOLTAGE SAG CONDITIONS

The IG-WTs are very sensitive to grid voltage sags, as the stator of the generator is directly connected to the

978-1-4244-5393-1/10/$26.00 ©2010 IEEE

mains. Although there are different kind of sags [16], they all give rise to common problems in such machines [17] as: mechanical rotor overspeed, electromagnetic torque peaks/ripple and inrush stator currents.

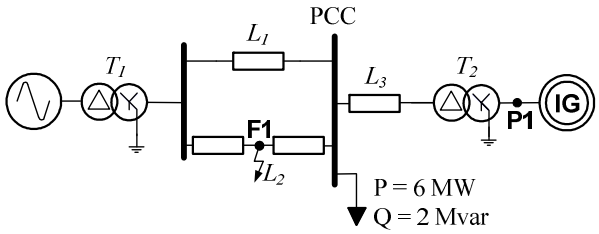

Fig.1.- Simulation platform for the analysis of a IG-WT under fault conditions.

In order to analyze the response of an IG-WT under fault conditions the distribution line depicted in Fig. 1 has been simulated.

In this study case a 690V 2MW IG-WT is connected though a cable and two overhead lines to a 150kV distribution network. In this case the shortcircuit power of the network is equal to 20MVA, ten times higher than the nominal power of the generator. In the figure *F1* depicts the fault point where the shortcircuit will be applied.

The simulation results that appear in Fig.2 and Fig.3 show the response of the system when a balanced fault (A type) and an unbalanced sag (C type) that appears at *F1* affects its stator windings [18].

A. Electromagnetic torque

Fig.2(a) describes the electromagnetical torque behavior of the IG when both faults occur. This variable experiences an important reduction during the fault period in all cases, due to the variation of the magnetic flux in the generator. Nevertheless, this torque drop is even more critical for the symmetrical fault than for the non-symmetrical one, as it can be noticed in the figure. However, the non-symmetrical voltages of the C sag produce an important torque ripple, due to the circulation of a negative sequence magnetic flux in the airgap. Once the faults are cleared, the average torque for the C sag still remains above the A sag value.

B. Speed of the rotor

Fig.2(b) shows the mechanical acceleration of the generator. During the fault period the input torque, provided by the wind, accelerates the machine's rotor. This acceleration is even higher when the A type sag appears, as the resistive electromagnetic torque is lower than in the C sag case. In this simulation the fast acceleration experienced by the rotor during the A sag drives the system to a mechanical unstable point. The performance of the graph, after the fault clearance, is an evidence of this situation, as the speed of the rotor keeps increasing out of control. These undesirable operating conditions, that could force the disconnection of the IG-WT, normally appear when there is a severe grid fault, and constitute a great problem for this kind of WTs. In spite of the stable behavior of the IG-WT obtained in the C sag simulation, this kind of faults are also able to drive these facilities to such unstable conditions depending on the sag's parameters.

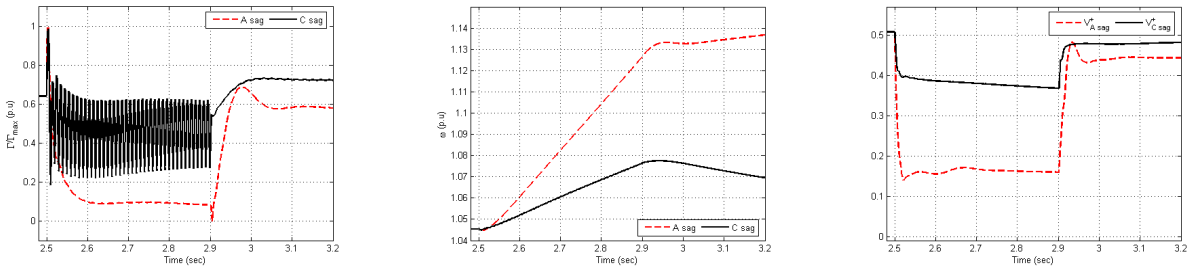

(a) (b) (c)

Fig. 2: Response of an induction generator in front of two different voltage dips, A (dashed line) sag and C sag (continuous line).(a)-Electromagnetic torque of the IG ; (b)-Mechanical speed of the rotor ; (c)- Positive sequence voltage at the IG. In both cases the fault appears at t=2.5s and is cleared at t=2.9s

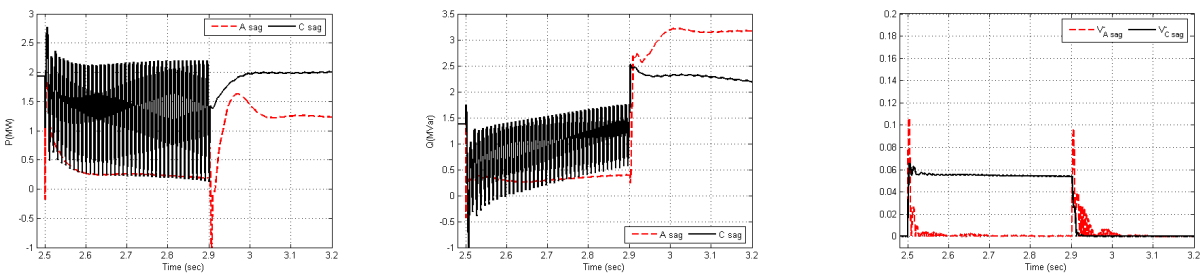

(a) (b) (c)

Fig. 3: Power and negative sequence voltage performance of a IG in front of two different voltage dips, A (dashed line) sag and C sag (continuous line).(a)-Active power delivered by the IG-WT during the fault and post fault periods ; (b)-Reactive power delivered by the IG-WT during the fault and post fault periods ; (c)- Negative sequence voltage at the stator windings. In both cases the fault appears at t=2.5s and is cleared at t=2.9s

C. IG's positive sequence voltage

In Fig.2(c) the positive sequence voltages at the IG terminals, at P1, are plotted. In this figure it stands out how the overall voltage reduction is higher when an A sag appears, due to the fact that all phases are short-circuited
to ground. At the same time it is also remarkable that, in both simulations, the nominal voltage magnitude is not retrieved instantaneously when the fault is cleared. This feature is against the stability of the system, as a slow recovery of the nominal voltage contributes to accelerate the machine after the fault.

D. Active and reactive power delivery

The performance of the active power delivered to the grid by the SCIG is detailed in Fig.3(a). This graph show how the injected power during the fault period is reduced with respect the nominal magnitude in both sags. The lowest average value, during and after the fault, is reached when the A sag is applied. In turn, the electromagnetic torque ripple that appeared in Fig.2(a) for the C sag is translated into active power ripple as well.

In Fig.3(b) the post-fault reactive power peaks in both simulations is the most relevant characteristic. These overshoots are due to the flow of high reactive currents, which are demanded by the SCIG in order to recover the magnetic flux at the generator. These currents yields important voltage drops at the SCIG terminals when the sags are cleared Fig.2(c).

From the simulation results it can be concluded that the fault ride-through capability of a SCIG wind turbine depends strongly on the maximum slip that this generator is able to withstand without getting out of control. This is evidenced in Fig.2(b), where the A voltage dip drives the machine to such conditions that the rotor keeps accelerating until the appropriate overspeed protection would trip it.

The simulations have demonstrated as well that this phenomenon is directly linked to the voltage evolution when the fault is cleared. If this magnitude is not high enough after the fault the generator is unable to convert the mechanical power into electrical power, accelerating thus the WT.

III. Strategies for Reactive Power Delivering

As shown in [19], some strategies for delivering reactive power into the grid under unbalanced conditions give rise to the injection of non-sinusoidal currents, which imposes high dynamic requirements to the current controller, increases the voltage distortion at the point of common coupling and might originates grid resonances. In this section, other reactive control strategies, able to deliver reactive power by injecting sinusoidal currents into the grid, are reviewed and commented.

According to the instantaneous power theory, the instantaneous reactive power q delivered by a reactive current vector $\mathbf{i}_q$ interacting generic voltage vector $\mathbf{v}$, is given by:

$$q = \left| \mathbf{v} \times \mathbf{i}_q \right|, \tag{1}$$

However, the instantaneous reactive power can be also calculated as a dot product:

$$q = \mathbf{v}_\perp \cdot \mathbf{i}_q \tag{2}$$

where $\mathbf{v}_\perp$ is an ortogonal (90-degrees leaded) version of the original grid voltage vector $\mathbf{v}$. Since the positive- and negative-sequence components of the reactive current injected by the STATCOM must be properly controlled, it will be assumed from here on that this current vector consists of a positive- and a negative sequence components, i.e., $\mathbf{i}_q = \mathbf{i}_q^+ + \mathbf{i}_q^-$. If this unbalanced current vector is injected into an unbalanced grid, with $\mathbf{v} = \mathbf{v}^+ + \mathbf{v}^-$, the instantaneous reactive power can be written as:

$$q = \mathbf{v}_\perp^+ \cdot \mathbf{i}_q^+ + \mathbf{v}_\perp^- \cdot \mathbf{i}_q^- + \mathbf{v}_\perp^+ \cdot \mathbf{i}_q^- + \mathbf{v}_\perp^- \cdot \mathbf{i}_q^+ \tag{3}$$

A.- Positive-Negative-Sequence Compensation (PNSC)

In the *PNSC* strategy, the reactive power delivered to the grid results from the interaction between voltages and currents with the same sequence. Moreover, it is imposed as a condition that oscillations in the reactive power resulting from the interaction of voltages and currents with different sequences should be mutually cancelled, i.e.,

$$Q = \mathbf{v}_\perp^+ \mathbf{i}_q^{*+} + \mathbf{v}_\perp^- \mathbf{i}_q^{*-} \quad ; \quad 0 = \mathbf{v}_\perp^+ \mathbf{i}_q^{*-} + \mathbf{v}_\perp^- \mathbf{i}_q^{*+} \tag{4}$$

This strategy gives rise to sinusoidal current waveforms, even under unbalanced grid voltage conditions, being the reference currents calculated as follow:

$$\begin{aligned} \mathbf{i}_\mathbf{q}^* &= \mathbf{i}_\mathbf{q}^{*+} + \mathbf{i}_\mathbf{q}^{*-} = b^\pm \left(\mathbf{v}_\perp^+ - \mathbf{v}_\perp^- \right), \\ b^\pm &= \frac{Q}{|\,\mathbf{v}_\perp^+\,|^2 - |\,\mathbf{v}_\perp^-\,|^2}. \end{aligned} \tag{5}$$

In this strategy, the interaction between voltage and current components with different sequences does not give rise to average active power but to power oscillations at twice the fundamental of the utility frequency, i.e.,

$$\begin{aligned} p = \mathbf{v} \cdot \mathbf{i}_\mathbf{q}^* = &\underbrace{\mathbf{v}^+ \cdot \mathbf{i}_\mathbf{q}^{*+} + \mathbf{v}^- \cdot \mathbf{i}_\mathbf{q}^{*-}}_{0} + \\ &\underbrace{\mathbf{v}^+ \cdot \mathbf{i}_\mathbf{q}^{*-} + \mathbf{v}^- \cdot \mathbf{i}_\mathbf{q}^{*+}}_{\tilde{p}}. \end{aligned} \tag{6}$$

B.- Average Active-Reactive Control (AARC)

In the *AARC* strategy, the reference reactive current vector $\mathbf{i}_q^*$ is monotonously proportional to the in-quadrature voltage vector $\mathbf{v}_\perp$. That is,

$$\mathbf{i}_\mathbf{q}^* = \mathbf{i}_\mathbf{q}^{*+} + \mathbf{i}_\mathbf{q}^{*-} = B\ \mathbf{v}_\perp \quad ; \quad B = \frac{Q}{V_\Sigma^2} \tag{7}$$

In (7), the susceptance B is a constant since it is calculated from the collective rms value of the grid voltage, which is defined by:

$$V_\Sigma = \sqrt{\frac{1}{T}\int_0^T |\mathbf{v}|^2\, dt} = \sqrt{|\mathbf{v}^+|^2 + |\mathbf{v}^-|^2} \qquad (8)$$

The reference current vector of (8) has the same direction as the in-quadrature voltage vector $\mathbf{v}_\perp$, giving rise to no active power. However the reactive power consists of an average value equal to Q plus an oscillating term, at twice the grid frequency, that is:

$$q = \mathbf{v}_\perp \cdot \mathbf{i}_q^* = \frac{|\mathbf{v}|^2}{V_\Sigma^2} Q = Q + \tilde{q} = Q\left[1 + \frac{2|\mathbf{v}^+||\mathbf{v}^-|}{|\mathbf{v}^+|^2 + |\mathbf{v}^-|^2}\cos(2\omega t + \phi^+ - \phi^-)\right] \qquad (9)$$

where ϕ^+ and ϕ^- are the phase-angles of the positive- and negative-sequence and $\mathbf{v}^+$ and $\mathbf{v}^-$ are the symmetrical components of the voltage, respectively.

C.- Balanced Positive-Sequence Control (BPSC)

In the *BPSC* strategy, the injected reactive currents are perfectly balanced and monotonously proportional to the in-quadrature positive-sequence voltage vector, as the averaged positive-sequence susceptance B^+ is a constant as well, i.e.,

$$\mathbf{i}_\mathbf{q}^* = \mathbf{i}_\mathbf{q}^{*+} = B^+ \mathbf{v}_\perp^+ \quad ; \quad B^+ = \frac{Q}{|\mathbf{v}^+|^2} \qquad (10)$$

Under unbalanced grid faults, the instantaneous reactive power delivered to the grid differs from Q because of the interaction between the injected positive-sequence current and the negative-sequence component of the grid voltage, $\tilde{q}$.

$$q = \mathbf{v}_\perp \cdot \mathbf{i}_\mathbf{q}^* = \underbrace{\mathbf{v}_\perp^+ \cdot \mathbf{i}_\mathbf{q}^*}_{Q} + \underbrace{\mathbf{v}_\perp^- \cdot \mathbf{i}_\mathbf{q}^*}_{\tilde{q}} \qquad (11)$$

Likewise, the instantaneous active power delivered by the *BPSC* control strategy during an unbalanced grid fault can by calculated as

$$p = \mathbf{v} \cdot \mathbf{i}_\mathbf{q}^* = \underbrace{\mathbf{v}^+ \cdot \mathbf{i}_\mathbf{q}^*}_{0} + \underbrace{\mathbf{v}^- \cdot \mathbf{i}_\mathbf{q}^*}_{\tilde{p}} \qquad (12)$$

IV. Simulation Results

To validate the expressions obtained from the study conducted in §III, some simulations were performed using PSCAD/EMTDC. The algorithm to calculate the reference currents was implemented on the natural *abc* reference frame, so the orthogonal voltage vector was calculated by:

In the simulation case considered in this section, the STATCOM injected zero reactive current into the grid during the prefault period (Q^*=0) and, once the grid fault is detected, it injected the highest allowed reactive power (Q^*=Q_M) without overpassing a current limit (I_{lim}), which was set as a reference input in the simulation model. Fig. 4 shows a simplified diagram of the control structure used in these simulations. A fault detector is used to change the reactive power reference when a fault occurs.

The layout of the study case used in the following simulations is shown in Fig. 5. As it can be seen in the figure a 10Mvar STATCOM was connected to ac collector of a 30MVA wind power plant (WPP), through a 33kV/690V transformer, T_2. Finally both, the WPP and the STATCOM, are connected to the electrical system through a second 120kV/33kV transformer, T_1. The connection of the WPP to the distribution network is carried out through two parallel lines, L_1//L_2.

To test the effectiveness of the proposed reactive current control strategies, a line-to-ground fault was considered at the half of L_2, which resulted in a type B dip, and after the *Y* winding of T_1, a type C dip. Finally, at the *Y* winding of T_2 a type D dip was obtained [20].

The positive- and negative-sequence voltage phasors during the fault were $\mathbf{V}^+ = 0.84\underline{|0^o}$ and $\mathbf{V}^- = 0.16\underline{|58^o}$, being the pre-fault voltage equal to $V_{pf}^+ = 1\underline{|0^o}$ p.u.. As stated before, the rated power of the simulated STATCOM was 10Mvar, the 30% of the wind farm nominal power, giving rise to a maximum rms line current equal to 8.367 kA. Therefore, in order to avoid overcurrents a current limit was set to I_{lim} = 11.833 kA ($\sqrt{2} \cdot 8.367$) at the STATCOM's output.

The simulated results, obtained with each control strategy, are shown in Fig. 6. It is worth to notice that all the control algorithms have been implemented in order to keep all currents under the nominal limit I_{lim}, shown in Fig 6 with a dotted line.

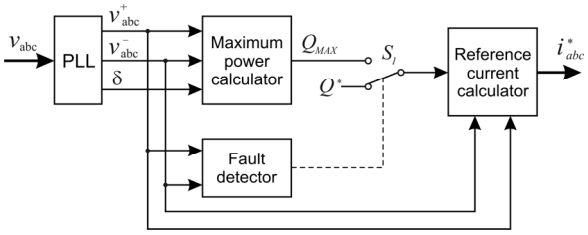

Fig. 4 Simplified diagram of the STATCOM control structure.

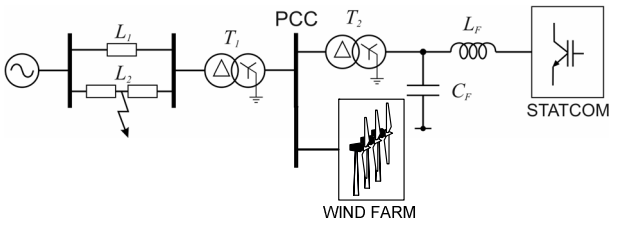

Fig. 5 Electrical scheme of the wind power plant considered in simulation.

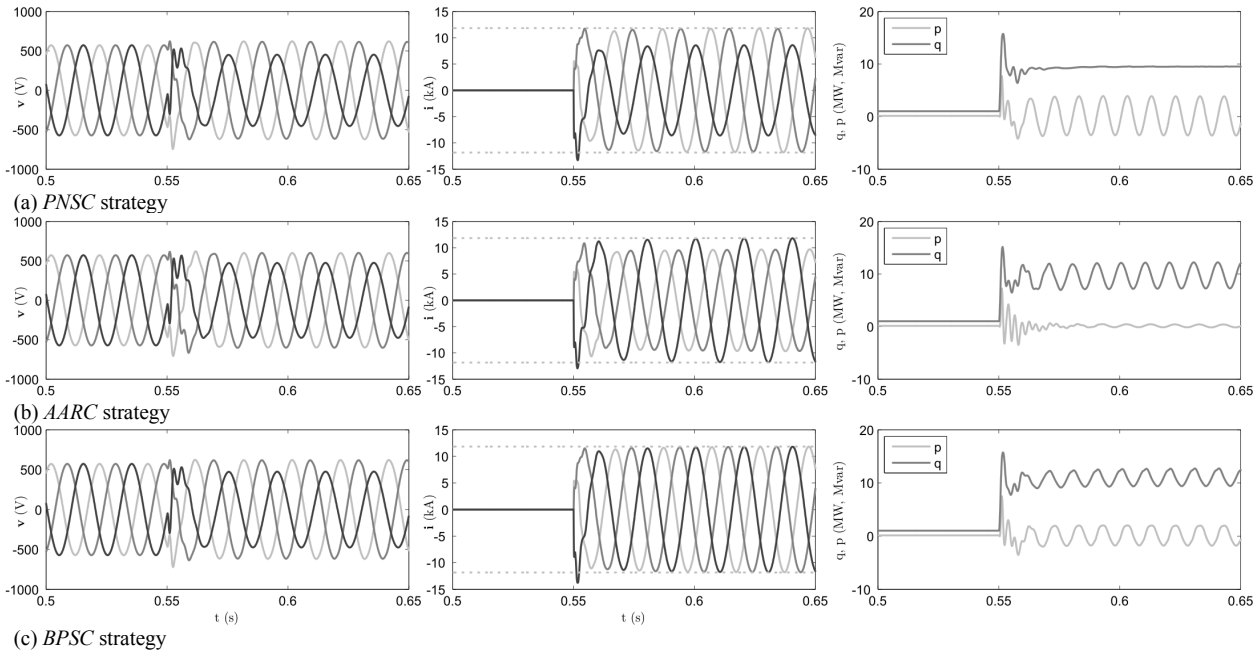

(a) *PNSC* strategy

(b) *AARC* strategy

(c) *BPSC* strategy

Fig. 6 – Simulation results. Columns from left to right: grid voltage, injected currents and the converter current limit, instantaneous active and reactive power delivered to the grid.

In the implementation of all the three strategies it is possible to realise how, after a transient period needed by the grid synchronization system to detect the grid voltage symmetrical components, the injected reactive currents are perfectly sinusoidal for all the three proposed strategies.

In these simulations, during a short transient, the phase currents slightly overpass the current limit during very short periods. However, the injected currents are always under control under steady state conditions. These short peaks are due to the high bandwidth of the STATCOM controller and the small link filter used in this simulation.

Regarding the power injected into the network, the plots representing the instantaneous powers in Fig. 6 corroborate that the *PNSC* strategy cancels out any oscillation in the injected reactive power resulting from the interaction of voltages and currents with different sequences. However, as expected from (6), this strategy give rise to oscillations in the delivered instantaneous active power, which implies oscillations in the dc-bus voltage.

On the other hand the *AARC* strategy does not generate dc-bus voltage oscillations since it does not deliver any active power. However, the injected reactive power presents some oscillations.

Finally, in the case of the *BPSC* strategy, the injected currents are perfectly sinusoidal with only positive sequence during the grid fault, which gives rise to oscillations in both the active and reactive power.

A.- Grid Voltage Support at the PCC

According to the maximum current that can be delivered by the 10MVAr STATCOM different reactive power levels can be injected, in function of the control strategy implemented at the STATCOM.

As a consequence, the capability for supporting the network voltage at the PCC changes between the *PNSC*, the *AARC* and the *BPSC*.

In order to analyze this difference the positive and negative sequence voltage has been measured at the PCC of Fig. 5, as well as the total reactive power injected in each case. The average values obtained in the test are summarized in TABLE I, where the characteristics values have been measured during a one-phase to ground fault as well.

TABLE I
PERFORMANCE OF VOLTAGE AT THE PCC WITH SCR=10

Strategy	**Q(MVAr)**	**PCC (p.u)**		
		V^+	**V^-**	**ΔV^+(%)**
NONE	0	0.6185	0.091	
PNSC	-9.37	0.6697	0.098	5.934
AARC	-9.46	0.6684	0.086	5.982
BPSC	-10.54	0.6739	0.091	6.112

TABLE I indicates that the BPSC strategy is the one that is able to inject the highest reactive power. This feature, together with the sole injection of positive sequence makes this value the highest among the tested strategies. On the other hand the PNSC and the AARC are able to inject less Q, due to the fact it should be limited as the resulting currents are unbalanced and hence the current limit is reached faster. However, both permit to reduce the negative sequence voltage. This is an interesting feature, as reducing this value permits to reduce the electromagnetic torque ripple in the generator,

what it can be advantageous for reducing the fatigue in the shaft. This feature is not compatible with the BPSC strategy, as no negative sequence currents are injected.

The performance of the STATCOM under the same operating conditions have been reproduced with a higher shortcircuit ratio (SCR) than the one used previously.

TABLE II
PERFORMANCE OF VOLTAGE AT THE PCC WITH SCR=20

Strategy	Q(MVAr)	PCC (p.u)		
		V^+	V^-	$\Delta V^+(\%)$
NONE	0	0.6198	0.090	
PNSC	-9.16	0.6550	0.095	5.712
AARC	-9.25	0.6542	0.086	5.760
BPSC	-10.31	0.6581	0.091	5.889

The results obtained in this test give rise to the same behaviour regarding the voltage components. However, the influence of the STATCOM in the performance of the voltage is lower in all cases, due to the minor impedance of the network.

V. EXPERIMENTAL RESULTS

The proposed reactive current control strategies were evaluated in an experimental setup shown in Fig. 7. The STATCOM was connected to the grid through a Δy transformer. The STATCOM consisted of a current-controlled VSI and a LC link filter connected. The grid consisted of another transformer with several taps. In the experiments, the grid fault was simulated by switching between two taps of the grid transformer, which gave rise to a voltage sag of 50% on phase *c*. This single-phase fault (type B dip) was propagated to the y winding of the transformer, giving rise to a type C sag. A dSpace 1103 DSP card was used to implement the reactive current injection strategies, the current limiter controller, the FLL and the low level resonant current controllers. The sampling and the switching frequencies in the experiments were set to 10 kHz and 20 kHz, respectively.

As a difference with the previous simulation results, the experimental test were carried out considering that the STATCOM was injecting the maximum level of reactive current during the before the fault. The current limit for the STATCOM in these experiments was set to 5A.

Figures 8(a), 8(b) and 8(c) show the grid voltages and the currents injected by the STATCOM for each control strategy. In these figures, the current scale is of 1A/V. Figures 8(d), 8(e) and 8(f) show the instantaneous active and reactive powers associated to previous voltage and currents waveforms.

In Figures 8(a), 8(b) and 8(c) it can be noticed the excellent performance of the proposed control strategies. In all cases the reactive currents injected by the STATCOM do not overpass the current limit.

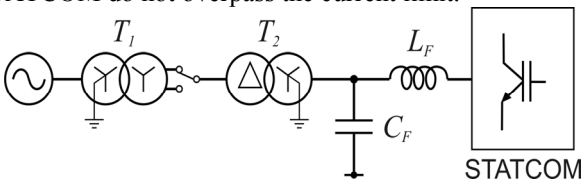

Fig. 7 Experimental setup used for testing the proposed control strategies.

The dynamics of the experimental STATCOM is slightly slower that the one considered in simulation, as the bandwidth of the controller were slightly reduce. This feature can be noticed in Figures 8(d), 8(e) and 8(f), where the instantaneous power presents a longer settle time before reaching steady state conditions during the grid fault.

It is worth to remark the excellent performance of the grid synchronization system, which is able to detect the new grid conditions during the faults in around one grid cycle. Moreover, it is also necessary to highlight the good performance of the resonant controllers used in the experimental setup, which allow tracking the sinusoidal reference, what consequently give rise to current waveforms and instantaneous powers that match perfectly the ones obtained in simulation.

VI. CONCLUSIONS

This paper presented three reactive current control strategies to achieve an effective and safe operation of a STATCOM during unbalanced grid faults.

The algorithms, for calculating the reference currents in the proposed control strategies were deduced using a generic space vector approach and the different terms, average and ripple, of the reactive power to be injected into the grid..

The proposed control strategies were implemented in simulation to control a STATCOM operating in a WPP by using PSCAD/EMTDC. Unbalanced faults were generated in the lines connecting the WPP. The results obtained from these simulations validated the effectiveness of the different strategies for controlling the STATCOM in a safe mode under unbalanced grid conditions.

The simulated results show that the injected currents are completely sinusoidal. However, the unbalance ratio depends upon the selected strategy. The BPSC is capable of injecting the highest reactive power, boosting the positive sequence to the highest value, and hence providing a major contribution to support the IG-WT during the fault. However the PNSC and the AARC are able to interact with the negative sequence, reducing thus the torque ripple.

The proposed reactive current control strategies were also evaluated by using an experimental setup. The experimental test carried out in the lab gave rise to satisfactory results that corroborated the excellent performance of the STATCOM under unbalanced grid

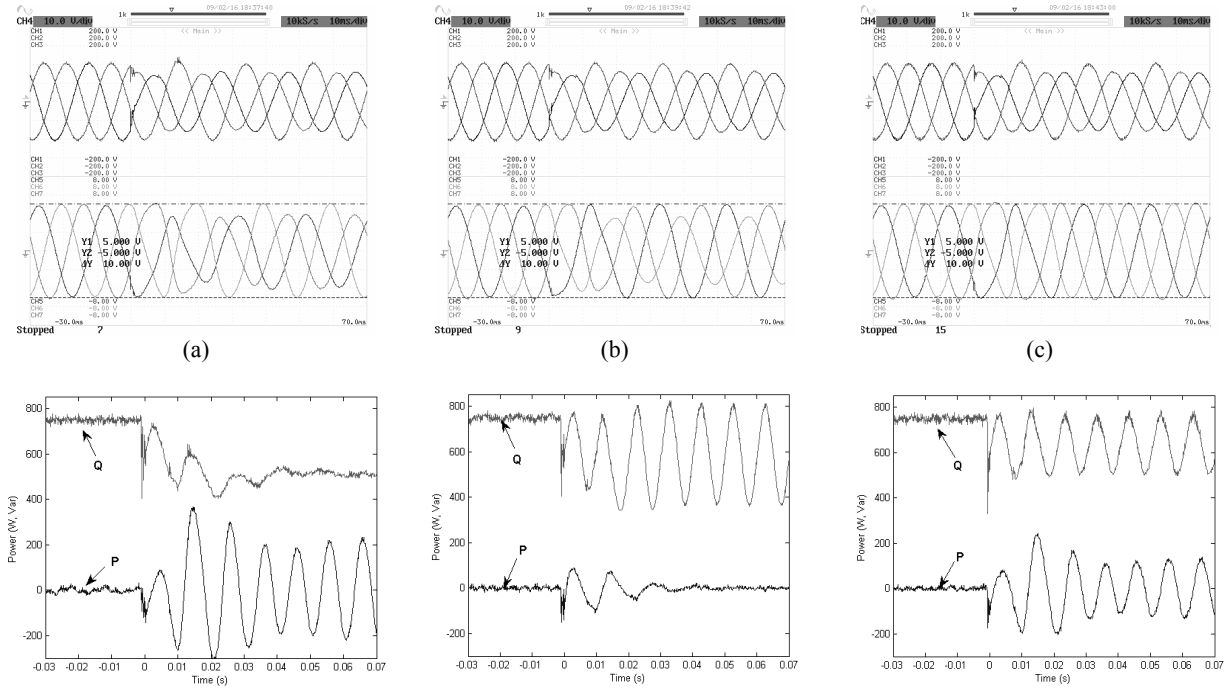

Fig. 8 Experimental results. (a) Grid voltages and currents for PNSC, (d) Active and reactive power for PNSC, (b) Grid voltages and currents for AARC, (e) Active and reactive power for AARC, (c) Grid voltages and currents for BPSC, (f) Active and reactive power for BPSC.

conditions when the proposed strategies were implemented.

REFERENCES

[1] E. Acha, V. Agelidis, O. Anaya-Lara and T.J. Miller, "Power Electronics Control in Electrical Systems", Newnes, 2002, ISBN 0-7506-5126-1.

[2] L. Gyugyi, "Dynamic compensation of AC transmission lines by solid-state synchronous voltage sources," IEEE Trans. on Power Delivery, vol.9, no.2, pp.904-911, Apr 1994

[3] L.Kuang, L. Jinjun, W. Zhaoan, W. Biao, "Strategies and Operating Point Optimization of STATCOM Control for Voltage Unbalance Mitigation in Three-Phase Three-Wire Systems," IEEE Trans. on Power Delivery, vol.22, no.1, pp.413-422, Jan. 2007.

[4] A. Edris, "FACTS technology development: an update," IEEE Power Engineering Review, vol.20, no.3, pp.4-9, Mar 2000.

[5] C. Han; Z. Yang, B. Chen, A.Q. Huang, Z. B. Zhang, M.R. Ingram, A.-A. Edris, "Evaluation of Cascade-Multilevel-Converter-Based STATCOM for Arc Furnace Flicker Mitigation," IEEE Tran. on Ind. Applicat., vol.43, no.2, pp.378-385, March-april 2007.

[6] A. Jain, K. Joshi, A. Behal, N. Mohan, "Voltage regulation with STATCOMs: modeling, control and results," IEEE Trans. On Power Delivery, vol.21, no.2, pp. 726-735, April 2006.

[7] C. Han, A.Q. Huang, M.E. Baran, S. Bhattacharya, W. Litzenberger, L. Anderson, A.L. Johnson, A.-A. Edris, "STATCOM Impact Study on the Integration of a Large Wind Farm into a Weak Loop Power System," IEEE Trans. on Energy Conversion, vol.23, no.1, pp.226-233, March 2008

[8] "Grid Code. High and extra high voltage", E.ON Netz GmbH, Germany, Apr. 2006.

[9] "Grid connection of wind turbines to networks with voltages above/below 100 kV", Energinet, regulations TF 3.2.5/TF 3.2.6, Denmark, Dec. 2004/May 2004.

[10] "Response requirements for electricity production facilities under special regulation in the presence of voltage sags,"(in Spanish), REE, PO 12.3, Spain, Oct. 2006.

[11] M. Molinas, J. Are; T. Undeland, "Low Voltage Ride Through of Wind Farms With Cage Generators: STATCOM Versus SVC," IEEE Trans. on Power Electronics, vol.23, no.3, pp.1104-1117, May 2008

[12] EWEA, "Large scale integration of wind energy in the european power supply: analysis, issues and recommendations." European Wind Energy Association (EWEA), Tech. Rep., 2005.

[13] I. Erlich, W. Winter, and A. Dittrich, "Advanced grid requirements for the integration of wind turbines into the german transmission system," in Power Engineering Society General Meeting, 2006. IEEE, 18-22 June 2006, p. 7pp.

[14] www.dena.de, "Planning of the grid integration of wind energy in germany onshore and offshore up to the year 2020 (dena grid study)," Dena - German Energy Agency, Tech. Rep., 2005.

[15] C. Hochgraf, R.H. Lasseter, "Statcom controls for operation with unbalanced voltages," IEEE Trans. on Power Delivery, vol.13, no.2, pp.538-544, Apr 1998.

[16] M. Bollen, "Voltage sags in three-phase systems," Power Engineering Review, IEEE, vol. 21, no. 9, pp. 8–11,15, Sept. 2001.

[17] L. Guasch, F. Corcoles, and J. Pedra, "Effects of symmetrical and unsymmetrical voltage sags on induction machines," Power Delivery, IEEE Transactions on, vol. 19, no. 2, pp. 774–782, April 2004.

[18] L. Zhang and M. Bollen, "Characteristic of voltage dips (sags) in power systems," Power Delivery, IEEE Transactions on, vol. 15, no. 2, pp. 827–832, 2000.

[19] Rodriguez, P.; Timbus, A.; Teodorescu, R.; Liserre, M.; Blaabjerg, F.; , "Reactive Power Control for Improving

Wind Turbine System Behavior Under Grid Faults," Power Electronics, IEEE Transactions on , vol.24, no.7, pp.1798-1801, July 2009

[20] M.H.J. Bollen and L.D. Zhang, ”Different methods for classification of three-phase unbalanced voltage dips due to faults,” Electric Power Systems Research, vol. 66, num. 1, pp. 59-69, July 2003.